*Progress In Electromagnetics Research M, Vol. 92, 213–221, 2020*

# Millimeter-Wave Ultra-Wideband PCB 180° Hybrid for 12–67 GHz

**Carl Pfeiffer[1, *], Thomas Steffen[1], and Boris Tomasic[2]**

**Abstract**—A myriad of ultra-wideband (UWB) 180° hybrids have been reported that operate at frequencies below 20 GHz. However, parasitics from printed circuit board (PCB) transmission lines become significantly more problematic as the frequency is extended to mm-wave frequencies. Here, a broadside coupled transmission line hybrid is investigated for operation at 12–67 GHz. It is shown that a parasitic time delay for the odd mode exists at the junction between coupled and uncoupled transmission lines. A heterogeneous multi-layer PCB stack-up is leveraged to compensate for the junction parasitics over an ultra-wide bandwidth. Measurements have an insertion loss between 2 and 12 dB across the band, $< 1.5$ dB amplitude balance, $< 10°$ phase balance, and $> 19$ dB isolation.

## 1. INTRODUCTION

A 180° hybrid coupler is a classic microwave circuit component that can be used to split an incident signal into in-phase ($\Sigma$) or out-of-phase ($\Delta$) signals [1]. These hybrids are sometimes referred to as magic-tees. They are used in a myriad of microwave circuits such as antenna feed networks, phase shifters, balanced mixers, and push-pull amplifiers. Narrowband hybrids are commonly realized using rat-race circuits. The bandwidth has been extended to one octave by cascading rat-race couplers [2]. However, there is a continual desire to increase bandwidth even further. There are two main approaches for realizing UWB 180° hybrids with bandwidths greater than one octave: a combination of a tee power splitter and a balun [3–9], or asymmetrically coupled transmission lines [1, 10]. Both of these approaches achieve perfect phase and amplitude balance over an ultra-wide bandwidth in theory. However, transmission line parasitics can significantly degrade performance in practice, especially as the frequency is increased. Therefore, a significant focus in high frequency UWB hybrid coupler design is compensating unwanted transmission line parasitics [11, 12].

Numerous 180° UWB hybrid couplers have been reported in the open literature that operate below 20 GHz. There also exist many mm-wave hybrids with less than 2 : 1 bandwidth ratios in the open literature [13–15]. However, the authors were unable to find any published 180° hybrids with more than one octave bandwidth that operate above 26 GHz. It should be noted that although the design details are not reported, UWB 180° hybrid couplers are commercially available up to 40 GHz [16–18]. Clearly, there are few examples of wideband 180° hybrid couplers that operate at mm-wave frequencies, and it is useful to investigate the achievable performance using PCB fabrication.

There also exist significant research efforts to develop narrowband miniaturized hybrids constructed with printed circuit boards (PCBs) [19–21] and monolithic microwave integrated circuits (MMIC) technology [2, 15, 22–24]. It should also be noted that MMIC 90° hybrids with wide bandwidths have been reported at mm-wave frequencies [25–28]. However, it is generally not possible to use a 90° hybrid design for inspiration when developing a 180° hybrid since the topologies and design methodologies for 180° and 90° hybrids are quite different.

*Received 3 March 2020, Accepted 7 May 2020, Scheduled 22 May 2020*

* Corresponding author: Carl Pfeiffer (carlpfei@umich.edu).

[1] Defense Engineering Corporation, 2458 Dayton Xenia Rd, Beavercreek, OH 45434, USA. [2] Air Force Research Laboratory, Sensors Directorate, 2241 Avionics Circle Wright-Patterson Air Force Base, OH 45433, USA.

Here, an ultra-wideband hybrid is reported that operates from 12–67 GHz, which covers the upper frequency limit of the commonly used 1.85 mm connector This work is an extension of [29] which mentioned the basic concept, but few results were reported. A heterogeneous multi-layer PCB stack-up is leveraged to compensate for the junction parasitics over an ultra-wide bandwidth. A similar approach was reported in [11], which used an air gap between coupled transmission lines to compensate for fringing capacitances and increase the operating frequency to 26 GHz. However, there was no explanation for how the air gap compensates fringing fields in [11]. Here, the junction is studied in more detail. It is clearly shown that the junction between coupled and uncoupled lines introduces a parasitic time delay for the odd mode, which can be compensated by designing a transmission line with different even and odd mode propagation constants. The hybrid is fabricated, and the measured performance is compared to the state-of-the-art.

## 2. DESIGN AND SIMULATION

Perhaps the most common UWB 90° and 180° hybrids are based on coupled transmission lines. These couplers can provide a decade or more bandwidth. The main difference between 90° and 180° hybrid couplers is that 90° hybrids use symmetrically coupled transmission lines, whereas 180° hybrids use asymmetric coupled transmission lines. The basic principle of the 180° hybrid operation is illustrated in Figure 1(a) [10]. Consider exciting the $\Delta$ port. The signal flows on a trace that is coupled to the trace from Port $B$. The two traces are adiabatically coupled to minimize reflection. Once coupled, the signal can be decomposed into even and odd modes with equal amplitudes. The impedances of the even and odd modes are $Z_0/k$ and $Z_0 k$, respectively, where $0 < k < 1$ is the coupling factor between the transmission lines. At the junction between the coupled and uncoupled lines, part of the signal is reflected. The even and odd modes are reflected with equal amplitude and 180° phase difference, which couples all of the reflected power into Port $B$. The transmission coefficients of the even and odd modes are equal, and all of the transmitted power flows into Port $A$. Similar arguments can be used to analyze the operation when excited at the other ports [10]. Typically, it is difficult to obtain sufficiently high transmission line coupling to generate a 3 dB coupler with a single junction. Therefore, the coupling is often set to 8.34 dB and two of these sections are connected in tandem to realize a 3 dB coupler, as shown in Figure 1(b) [30, 31].

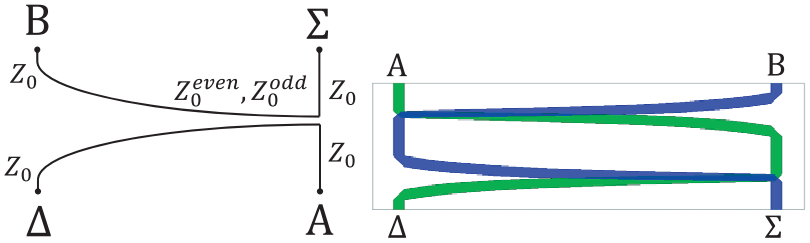


**Figure 1.** (a) Schematic of an asymmetrically coupled transmission line. (b) Offset stripline implementation of a broadside coupled transmission line hybrid. Two 8.34 dB couplers are cascaded together to realize a 3 dB, 180° hybrid coupler.

Coupled line hybrids often employ an offset stripline topology, which offers high transmission line coupling and nondispersive propagation. In theory, the bandwidth of the asymmetrically coupled transmission lines is limited only by the ability to provide a broadband impedance match from uncoupled to coupled transmission lines. However, there always exist parasitic reactances at the junction between the coupled and uncoupled transmission lines. These parasitics introduce additional phase shifts in the reflected and transmitted signals, which creates phase and amplitude imbalance. An example junction between coupled and uncoupled lines is shown in Figure 2. The top and bottom ground planes are transparent for clarity and the relative permittivity of the substrate is $\varepsilon_r = 3.5$. The transmission and reflection coefficients of the junction are shown in Figure 3. As the frequency is reduced the reflection

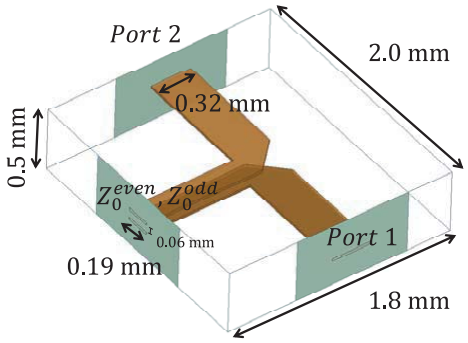


**Figure 2.** Junction between coupled transmission lines ($Z_0^{even}$ and $Z_0^{odd}$) and uncoupled transmission lines (Port 1 and Port 2).

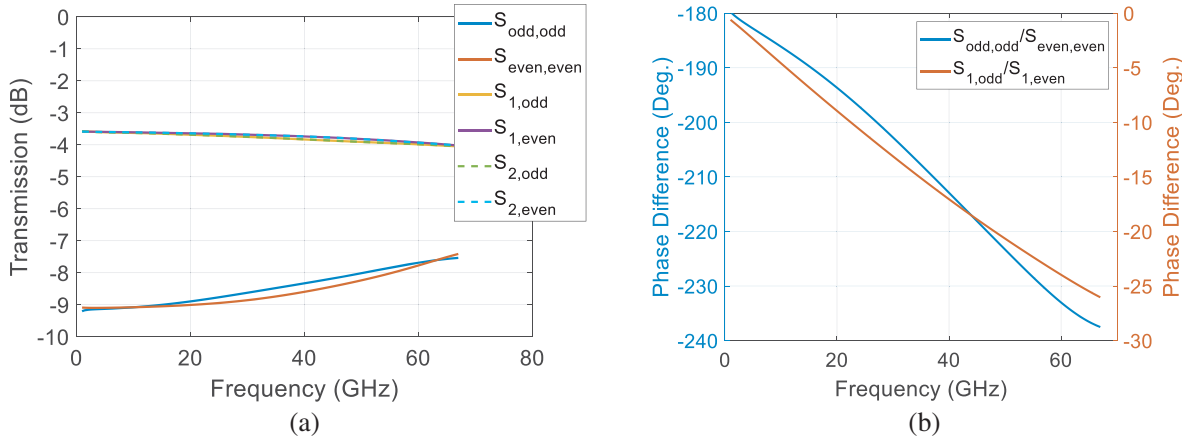


**Figure 3.** Transmission and reflection coefficients of the different ports/modes of the junction shown in Figure 2. (a) Amplitude and (b) phase difference.

and transmission phase difference of the even and odd modes approaches the ideal case of 180° and 0° respectively (see Figure 3(b)).

At higher frequencies the reflected and transmitted phase differences are far from 180° and 0°. Different methods of reducing the impact of parasitics have been proposed [11, 12, 32, 33]. However, no examples have been reported that compensate for these parasitics at mm-wave frequencies. An equivalent circuit for the junction parasitics is reported in [33]. There is a mutual capacitance and inductance between the coupled transmission lines at the junction, which introduces an additional time delay for the odd mode relative to the even mode. The time delay difference between the odd and even modes is also observed in full wave simulations (e.g., Figure 3(b)). The length of this delay typically corresponds to half the width of the uncoupled transmission lines (0.17 mm here), which translates into 25° phase error at 67 GHz for the transmission coefficient from the even and odd modes to the uncoupled lines.

The goal is to compensate for the increased delay of the odd mode at the junction. To accomplish this, two different dielectric substrates are used in the compensated stripline design shown in Figure 4. A substrate with $\varepsilon_r = 3.0$ is sandwiched between two other substrates with $\varepsilon_r = 3.5$. When the odd mode is excited, the field is concentrated between the coupled transmission lines, which propagates at a faster group velocity relative to the even mode. By properly optimizing the length of the coupled transmission lines, the parasitic time delay at the junction is compensated. The transmission and reflection coefficients of the compensated junction are shown in Figure 5. The reflection and transmission ratios in Figure 5(b) are relatively constant vs. frequency with just 3.5° phase error across the band. The disadvantage of this approach is the required length of the adiabatically coupled transmission lines is a function of the

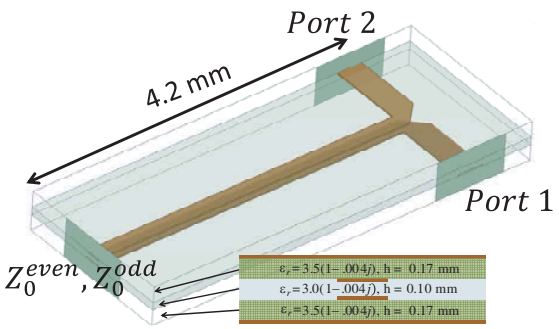


**Figure 4.** Heterogenous material stack-up of the offset stripline for compensating junction parasitics.

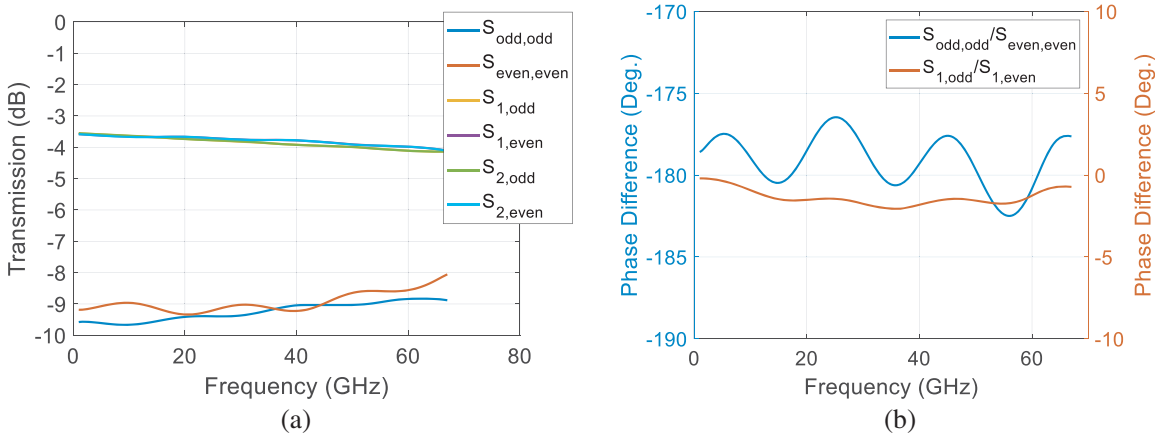


**Figure 5.** Transmission and reflection coefficients of the different ports/modes of the junction shown in Figure 4. (a) Amplitude and (b) phase difference.

substrate permittivities. Thus, a different material stack-up may be necessary if a different bandwidth is required. Note that there is also an amplitude imbalance since the coupling tends to increase at higher frequencies (see Figure 5(a)). This amplitude imbalance is on the order of 1 dB and is not compensated here, which does create some unwanted amplitude imbalance in the final design.

It should be noted that a similar approach is reported in [11] with a maximum operating frequency of 26 GHz. However, an air gap between the coupled transmission lines is employed in [11], which requires nonstandard PCB fabrication. Furthermore, [11] only states that the air gap compensates for fringing electric fields, but no additional explanation is provided.

A working hybrid requires several components in addition to the junction (e.g., adiabatically coupled transmission lines, bends, impedance tapers), which are optimized through manual tuning and a pattern search optimization in HFSS. A top view of the optimized design is shown in Figure 6(a) and the dielectric stack-up is shown in Figure 6(b). The exponential taper provides a broadband impedance match from the uncoupled stripline mode to the coupled lines. In addition, the length of the taper is optimized to compensate for the time delay at the junction. The linewidths of the transmission line are tapered between 0.32 mm in the uncoupled sections to 0.19 mm in the tightly coupled regions. It is necessary to add a meander to the transmission line connected to port $A$ to establish proper phase balance between the $A$ and $B$ ports [10]. A small meander is also added to the $B$ port transmission line to increase symmetry. The middle two layers of the hybrid have a gridded ground plane away from the signal traces. This gridded ground plane is added to improve the multilayer bonding processes used in fabrication. The grid is far enough away from the signal traces such that it does not affect the performance. The hybrid is fed with narrow block 1.85 mm microstrip end-launch connectors. The landing pads for these standard connectors occupy a significant percentage of the overall area. Wideband transitions between the offset stripline and microstrip sections are straightforward to design,

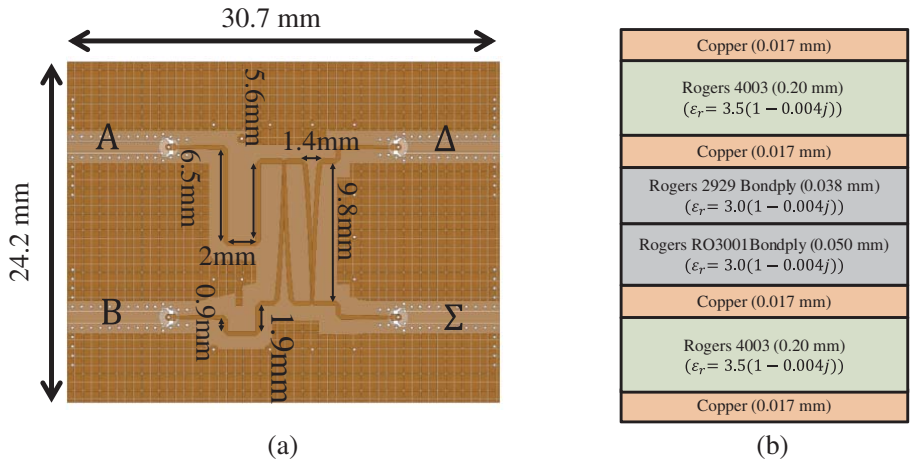


**Figure 6.** (a) Top view of designed coupled transmission line hybrid. (b) Material stack-up.

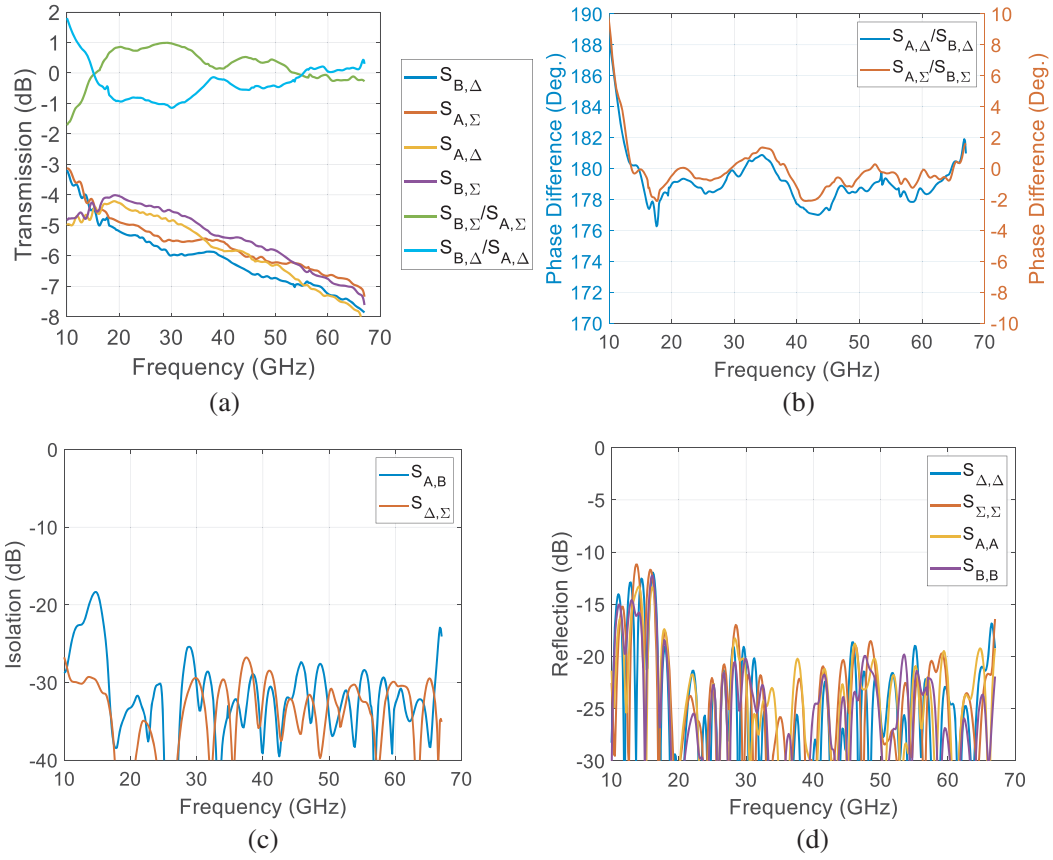


**Figure 7.** Simulated performance of the coupled line hybrid. (a) Transmission coefficients and amplitude balance. (b) Transmitted phase balance. (c) Isolation. (d) Reflection coefficients.

and therefore their details are not included here.

The simulated performance of the designed hybrid is shown in Figure 7. The amplitude and phase balance are less than ±1.1 dB and ±3°. The return loss is greater than 10 dB and isolation is greater than 19 dB across the band. The simulated insertion loss is 4.5 dB at 67 GHz, accounting for the 3 dB power split.

## 3. FABRICATION AND MEASUREMENTS

The coupled line hybrid is built using a commercial PCB fabrication vendor and standard PCB techniques. The dielectric stack-up is shown in Figure 6(b). The lower permittivity substrate in the middle of the stack-up is implemented with 90 µm thick Rogers Corp. 2929 bondply. The top and bottom core substrates are 200 µm thick Rogers Corp. 4003. The internal sides of the 4003 panels are first etched using photolithography. Then the substrates are bonded together. During the bonding process the bondply reflows and fills in any air gaps between the 4003 cores. Next, the through-hole vias are drilled and plated. The very top and bottom copper layers are then etched, and the surface is plated with electroless nickel immersion gold (ENIG) to protect the metal from corrosion. The fully assembled hybrid is shown in Figure 8. The narrow block 1.85 mm end launch connectors occupy a large percentage of the area.

The measured performance is shown in Figure 9. The amplitude balance is $< 1$ dB for the vast majority of frequencies (10–63 GHz) and is $< 1.5$ dB in the range of 7–67 GHz. The phase balance is less than 8° in the range of 16–67 GHz. The 7 dB return loss is somewhat high, and is also attributed to connector mismatch since the 1.85 mm end launch connectors were not accurately modelled. The insertion loss is 9 dB at 60 GHz, which is quite high. Further studies are needed to conclusively determine the source of the high measured loss, which could be due to surface roughness, increased dielectric loss tangent at mm-wave frequencies, radiation losses, etc. The measured performance of the proposed hybrid is compared to state-of-the-art 180° hybrids in Table 1. The proposed coupler has a similar bandwidth, amplitude balance, and phase balance as lower frequency hybrids. Note that [16–18] correspond to

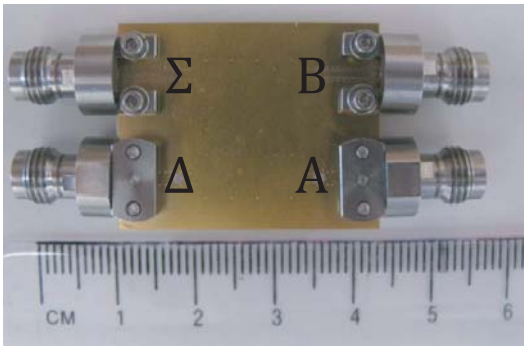


**Figure 8.** Fabricated hybrid coupler.

**Table 1.** Comparison of state-of-the-art UWB 180° hybrid couplers.

| Ref. | BW ratio | Max Freq. (GHz) | Max Amp. Imbalance | Max Phase Imbalance | Max Insertion Loss | Min Isolation | Size at lowest frequency | Fabrication Technology |
|---|---|---|---|---|---|---|---|---|
| [2] | 2 : 1 | 44 | 1 dB | 5° | 3.2 dB | 20 dB | $\lambda_L/15 \times \lambda_L/19$ | CMOS |
| [6] | 3.7 : 1 | 11 | 0.8 dB | 5° | 5 dB | - | $\lambda_L/2 \times \lambda_L/2.5$ | PCB |
| [11] | 13 : 1 | 26 | 1.2 dB | 5° | 2.5 dB | 15 dB | - | PCB |
| [12] | 10 : 1 | 18 | 2 dB | - | 1.5 dB | 15 dB | - | PCB |
| [16] | 2.2 : 1 | 40 | 1 dB | 8° | 2.5 dB | 16 dB | $1.4\lambda_L \times 1.7\lambda_L$ | - |
| [17] | 6.7 : 1 | 40 | 1.2 dB | 12° | 3 dB | 13 dB | $\lambda_L/1.2 \times \lambda_L/1.2$ | - |
| [18] | 4 : 1 | 40 | 1 dB | 12° | 1.7 dB | 15 dB | $\lambda_L/1.4 \times \lambda_L/1.1$ | - |
| [15] | 1.5 : 1 | 160 | 0.5 dB | 10° | 1.1 dB | 25 dB | $\lambda_L/9.3 \times \lambda_L/17$ | CMOS |
| **This Work** | **5.5 : 1** | **67** | **1.5 dB** | **10°** | **12 dB** | **18 dB** | $\mathbf{1.2\lambda_L \times 1.0\lambda_L}$ | **PCB** |

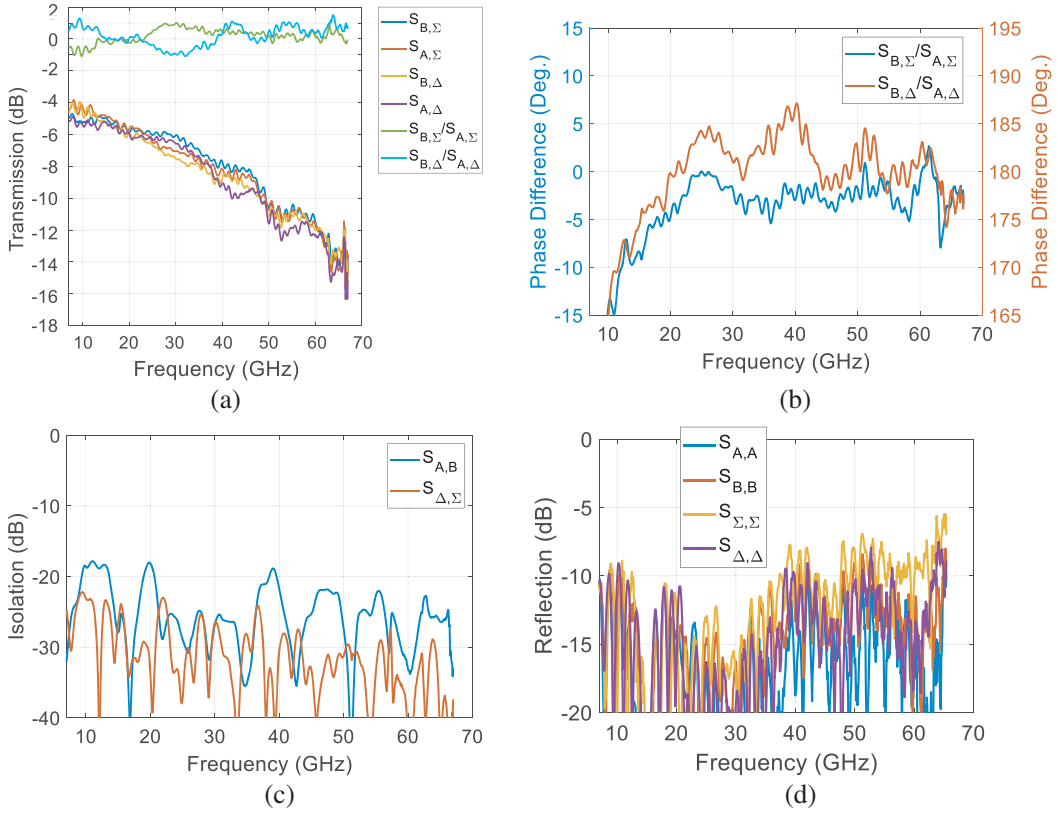


**Figure 9.** Measured performance of the coupled line hybrid. (a) Transmission coefficients and amplitude balance. (b) Transmitted phase balance. (c) Isolation. (d) Reflection coefficients.

commercially available hybrids, which do not provide any design details. The bandwidth is significantly larger than other mm-wave hybrids in the open literature.

## 4. SUMMARY

A UWB 180° hybrid coupler operating from 12–67 GHz is reported. Theory, design, and simulation results are presented. The coupled line hybrid is fabricated, and the measured performance is compared to state-of-the-art hybrids. This work presents design insights into compensating for transmission line parasitics at mm-wave frequencies, and also provides a baseline for future mm-wave 180° hybrid designs.

The current hybrid does suffer from high insertion loss though. One method of reducing insertion loss in the future is employing lower loss materials. For example, a similar hybrid design was fabricated using Teflon based substrates ($\varepsilon_r = 2.3(1 - 0.001j)$). The measured insertion loss of this design was reduced to 5 dB at 60 GHz. However, the features were less accurately fabricated, which resulted in increased amplitude and phase imbalance of 2.8 dB and 12°, respectively. This fact highlights the importance of finding a good tradeoff between substrates with low loss and accurate manufacturability.

## REFERENCES

1. Cohn, S. B. and R. Levy, "History of microwave passive components with particular attention to directional couplers," *IEEE Transactions on Microwave Theory and Techniques*, Vol. 32, 1046–1054, 1984.
2. Garay, E., M.-Y. Huang, and H. Wang, "A cascaded self-similar rat-race hybrid coupler architecture and its compact fully integrated Ka-band implementation," *IEEE/MTT-S Internation Microwave Symposium — IMS*, 79–82, Philadelphia, 2018.

3. Aikawa, M. and H. Ogawa, "Double-sided MICs and their applications," *IEEE Transactions on Microwave Theory and Techniques*, Vol. 37, 406–413, 1989.
4. Ho, C.-H., L. Fan, and K. Chang, "Broad-band uniplanar hybrid-ring and branch-line couplers," *IEEE Transactions on Microwave Theory and Techniques*, Vol. 41, 2116–2125, 1993.
5. Fan, L., C.-H. Ho, S. Kanamaluru, and K. Chang, "Wide-band reduced-size uniplanar magic-T, hybrid-ring, and de Ronde's CPW-slot couplers," *IEEE Transactions on Microwave Theory and Techniques*, Vol. 43, 2749–2758, 1995.
6. Scherr, S., S. Ayhan, G. Adamiuk, P. Pahl, and T. Zwick, "Ultrawide bandwidth-hybrid-coupler in planar technology," *International Journal of Microwave Science and Technology*, Vol. 2014, 486051, 2014.
7. Ang, K. S. and Y. C. Leong, "Converting baluns into broad-band impedance-transforming 180° hybrids," *IEEE Transactions on Microwave Theory and Techniques*, Vol. 50, 1990–1995, 2002.
8. Bialkowski, M. E. and Y. Wang, "Wideband microstrip 180° hybrid utilizing ground slots," *IEEE Microwave and Wireless Components Letters*, Vol. 20, 495–497, 2010.
9. Llamas, M. A., M. Ribo, D. Girbau, and L. Pradell, "A rigorous multimodal analysis and design procedure of a uniplanar 180° hybrid," *IEEE Transactions on Microwave Theory and Techniques*, Vol. 57, 1832–1839, 2009.
10. Pozar, D. M., *Microwave Engineering*, John Wiley & Sons, 2009.
11. Nakajima, M. and H. Tanabe, "A design technique for raising upper frequency limit of wide-band 180° hybrids," *IEEE MTT-S International Microwave Symposium Digest*, Vol. 2, 879–882, 1996.
12. Gruszczynski, S., K. Wincza, and K. Sachse, "Design of compensated coupled-stripline 3-dB directional couplers, phase shifters, and Magic-T's — Part II: Broadband coupled-line circuits," *IEEE Transactions on Microwave Theory and Techniques*, Vol. 54, 3501–3507, 2006.
13. Moghaddasi, J. and K. Wu, "Planar 180° hybrid couplers with non-interspersed ports for millimeter-wave applications," *Journal of Microwave and Wireless Technologies*, Vol. 12, 293, 2020.
14. Afroz, S. and K.-J. Koh, "W-band (92–100 GHz) phased-array receive channel with quadrature-hybrid-based vector modulator," *IEEE Trans. on Circuits and Systems — I: Regular Papers*, Vol. 65, 2070, 2018.
15. Hou, D., W. Hong, W. L. Goh, Y. Z. Xiong, and M. Annamalai, "CMOS hybrid couplers with improved phase inverter structure for D-band applications," *IET Microwaves, Antennas & Propagation*, Vol. 7, No. 7, 569, 2013.
16. RF-Lambda, Accessed January 2020, [Online]. Available: https://www.rflambda.com/pdf/hybrid/RFHB26G40GPI.pdf.
17. Pulsar, Accessed January 2020, [Online]. Available: https://www.pulsarmicrowave.com/product/180_degree_hybrid/JSO-51-471-6S.
18. Krytar, Accessed January 2020, [Online]. Available: https://krytar.com/pdf/4100400.pdf.
19. Sung, Y., C. Ahn, and Y.-S. Kim, "Size reduction and harmonic suppression of rat-race hybrid coupler using defected ground structure," *IEEE Microwave and Wireless Components Letters*, Vol. 14, 7–9, 2004.
20. Settaluri, R. K., G. Sundberg, A. Weisshaar, and V. Tripathi, "Compact folded line rat-race hybrid couplers," *IEEE Microwave and Guided Wave Letters*, Vol. 10, 61–63, 2000.
21. Ahn, H., I.-S. Chang, and S.-W. Yun, "Miniaturized 3-dB ring hybrid terminated by arbitrary impedances," *IEEE Transactions on Microwave Theory and Techniques*, Vol. 42, 2216–2221, 1994.
22. Chang, H.-Y., P.-S. Wu, T.-W. Huang, H. Wang, C.-L. Chang, and J. G. Chern, "Design and analysis of CMOS broad-band compact high-linearity modulators for gigabit microwave/millimeter-wave applications," *IEEE Transactions on Microwave Theory and Techniques*, Vol. 54, 20–30, 2006.
23. Li, T.-W., J. S. Park, and H. Wang, "A 2–24 GHz 360° full-span differential vector modulator phase rotator with transformer-based poly-phase quadrature network," *IEEE Custom Integrated Circuits Conference (CICC)*, 1–4, 2015.
24. Tseng, S.-C., C. Meng, C.-H. Chang, S.-H. Chang, and G.-W. Huang, "A silicon monolithic phase-inverter rat-race coupler using spiral coplanar striplines and its application in a broadband Gilbert

mixer," *IEEE Transactions on Microwave Theory and Techniques*, Vol. 56, 1879–1888, 2008.

25. Hamed, K. W., A. P. Freundorfer, and Y. M. M. Antar, "A new broadband monolithic passive differential coupler for K/Ka-band applications," *IEEE Transactions on Microwave Theory and Techniques*, Vol. 54, No. 6, 2527, 2006.
26. Chirala, M. K. and B. A. Floyd, "Millimeter-wave lange and ring-hybrid couplers in a silicon technology for E-band applications," *IEEE MTT-S International Microwave Symposium Digest*, 1547–1550, 2006.
27. Hou, Z. J., Y. Yang, L. Chiu, X. Zhu, and Q. Xue, "Wideband millimeter-wave on-chip quadrature coupler with improved in-band flatness in 0.13-µm SiGe technology," *IEEE Electron Device Letters*, Vol. 39, No. 5, 652, 2018.
28. Park, J. S. and H. Wang, "A transformer-based poly-phase network for ultra-broadband quadrature signal generation," *IEEE Transactions on Microwave Theory and Techniques*, Vol. 63, No. 12, 4444, 2015.
29. Pfeiffer, C., T. Steffen, and B. Tomasic, "UWB millimeter-wave 180 hybrid couplers," *IEEE International Symposium on Antennas and Propagation and USNC-URSI Radio Science Meeting*, 967–968, Atlanta, 2019.
30. Monteath, G. D., "Coupled transmission lines as symmetrical directional couplers," *Proceedings of the IEE — Part B: Radio and Electronic Engineering*, Vol. 102, 383–392, 1955.
31. Shelton, J. P. and J. A. Mosko, "Synthesis and design of wide-band equal-ripple TEM directional couplers and fixed phase shifters," *IEEE Transactions on Microwave Theory and Techniques*, Vol. 14, 462–473, 1966.
32. Gruszczynski, S. and K. Wincza, "Generalized methods for the design of quasi-ideal symmetric and asymmetric coupled-line sections and directional couplers," *IEEE Transactions on Microwave Theory and Techniques*, Vol. 59, 1709–1718, 2011.
33. Gruszczynski, S., K. Wincza, and K. Sachse, "Design of compensated coupled-stripline 3-dB directional couplers, phase shifters, and magic-T's — Part I: Single-section coupled-line circuits," *IEEE Transactions on Microwave Theory and Techniques*, Vol. 54, 3986–3994, 2006.